Halbach array linear alternator for thermo-acoustic engine

Saha, C. R. , Riley, P. H. , Paul, J. , Yu, Z. , Jaworski, A. J. and Johnson, C. M.

Original citation:
Saha, C. R. , Riley, P. H. , Paul, J. , Yu, Z. , Jaworski, A. J. and Johnson, C. M. (2012) Halbach array linear alternator for thermo-acoustic engine. Sensors and Actuators A: Physical, volume 178 : 179-187

http://dx.doi.org/10.1016/j.sna.2012.01.042

DOI: 10.1016/j.sna.2012.01.042
ISSN: 0924-4247

Publisher: Elsevier

Sensors and Actuators A 178 (2012) 179–187

Contents lists available at SciVerse ScienceDirect

Sensors and Actuators A: Physical

journal homepage: www.elsevier.com/locate/sna

Halbach array linear alternator for thermo-acoustic engine

C.R. Saha [a,*], Paul H. Riley [a], J. Paul [a], Z. Yu [b], A.J. Jaworski [b], C.M. Johnson [a]

[a] Department of Electrical and Electronic Engineering, The University of Nottingham, Nottingham NG7 2RD, UK
[b] Department of Engineering, The University of Leicester, University Road, Leicester LE1 7RH, UK

ARTICLE INFO

Article history:
Received 24 September 2011
Received in revised form 25 January 2012
Accepted 26 January 2012
Available online 4 February 2012

Keywords:
Alternators
Suspension loss
Thermo-acoustic
Resonance

ABSTRACT

This paper focuses on the design issues of a thermo-acoustically driven low-cost linear alternator for the SCORE project. SCORE (www.score.uk.com) aims to improve the quality of life around 2 billion poor people in the rural communities of the developing countries. The advantage of the double Halbach array permanent magnet moving coil alternator structure over traditional loudspeaker as a linear alternator is presented. The theoretical analysis of the linear alternator at different coil configurations with the rectifier circuit is explained and analysed with the finite elements simulation results. The simulation results show that the double coil structure with the smaller number of coil turns would be suitable for this project. The experimental results of the double Halbach array prototype which has been built and tested are discussed and compared with the simulation results.

1. Introduction

Around 2 billion people in the world live in rural communities in developing countries without electricity [1–3]. Most of the women in these communities cook their food for around 4 h per day over an open 3 stone fire and the smoke produced is extremely bad for their health. A Stove that does not produce smoke and generates electricity has been shown to be beneficial to them [4,5]. The SCORE Stove concept is to generate electricity from a cooking stove using a well-known thermo-acoustic principle [6–17]. Heat produces sound which is then converted to electricity using a linear alternator. The electricity can be stored in a battery for later use in such applications as lighting, charging mobiles phones or radios. Most of the commercially available linear alternators are piston type generators (used in free piston Stirling Engines) which are not suitable for the SCORE project in terms of cost and size [18–21]. Being targeted at the poor, low cost is a key element in the design, and conventional mass produced low-cost loudspeakers working in reverse can be used. Their efficiency is rather poor at 50%, and the suspensions are made from materials with high damping and limited mechanical stability [22]. However changing the design rules can preserve the low cost element and make considerable functional improvements when used as an alternator. Whereas a loudspeaker requires good linearity and defined electrical impedance to preserve sound quality over a large frequency range, a linear alternator is a fixed frequency device that can tolerate non-sinusoidal waveforms and requires high efficiency operation.

The SCORE linear alternator has a target cost of £4 [4] with a magnet assembly target of £3.30 for a 150 W unit. By utilising NdFeB permanent magnets in a Halbach array [23], considerable functional improvements can be made whilst preserving the low cost mass-produced manufacturing process. At the time of writing, a magnet supplier has estimated the price of NdFeB in very large quantities as around £70/kg, the maximum affordable magnet mass is therefore 0.047 kg. This paper addresses the design issues of the linear alternator for the SCORE project to meet the target cost and power. The next section introduces the cylindrical shape double Halbach array moving coil alternator design can be constructed without any additional magnetic material, such as soft iron or Si-iron laminations. It is well known that Halbach array magnetic flux can be enhanced on one side and cancelled on the other side and the fundamental advantage of the Halbach array machine is already explained in [24,25]. Fig. 1(a) shows a linear Halbach array which enhances flux density on one side with a low flux on the opposite side. Fig. 1(b) shows two Halbach arrays with the enhanced sides facing each other so that flux is highly concentrated in the gap. Losses in the circular, co-axial double Halbach array alternator as shown in Fig. 5 are from the coil internal resistance only. Being moving coil placed in the gap of maximum flux density, there is no conventional core loss and eddy current loss since the laminations or back iron do not exist and the moving element is lighter compared to a traditional moving iron or moving magnet machine. The following section describes the theoretical issues of the alternator coil design to understand the fundamental concepts of voltage and efficiency when used with a battery rectifier circuit. 2-D finite element simulation results of the double and multiple moving coil

* Corresponding author. Tel.: +44 11 58466890.
E-mail addresses: chitta.saha@nottingham.ac.uk, chittajd@yahoo.com (C.R. Saha).

0924-4247
doi:10.1016/j.sna.2012.01.042

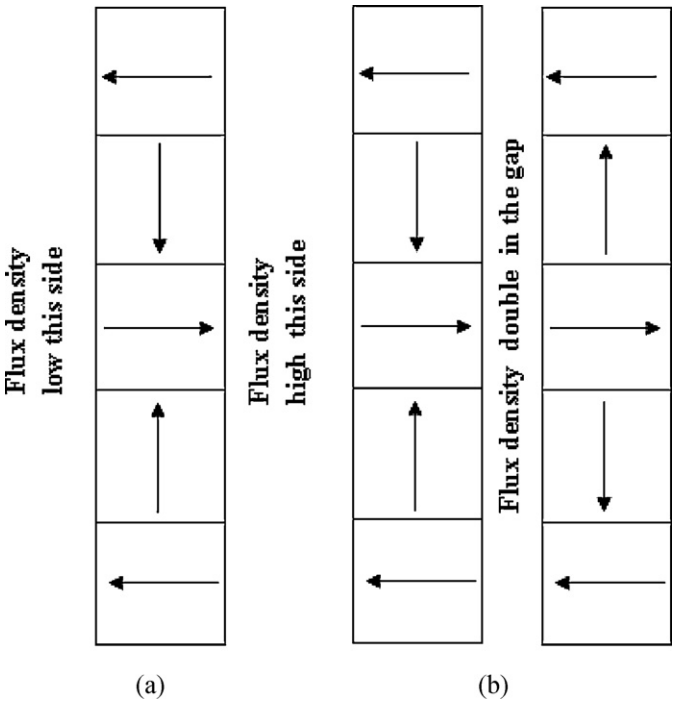

Fig. 1. (a) A five magnets single Halbach array (left) and (b) five magnets double Halbach array (right) structure.

configurations is shown and discussed. Finally the experimental result of the double Halbach array alternator which has been built and tested is presented in order to see the comparison with the simulation results.

2. Design consideration of the alternator

The output power and cost of the linear alternator is fixed for the SCORE project application and used as a basis for the electrical design. Magnet volume is defined by the cost target but the trade-offs between output power, operating frequency, coil displacement and efficiency of the thermo-acoustically driven linear alternator need to be addressed. Fig. 2 shows the schematic of a typical moving coil loudspeaker type alternator. The loudspeaker type alternator consists of a moving coil inside a static magnetic field where the voice coil is connected to the cone and its suspension. Normally the cone is made from carbon fibre, plasticized cloth or paper. The magnet assembly consists of front plate, back plate, yoke pole pitch which are mainly made from low cost iron material and a large ferrite magnet. The vent holes allow the air displaced by the coil to pass to the outside. An efficient thermo-acoustic linear alternator (see later) requires a

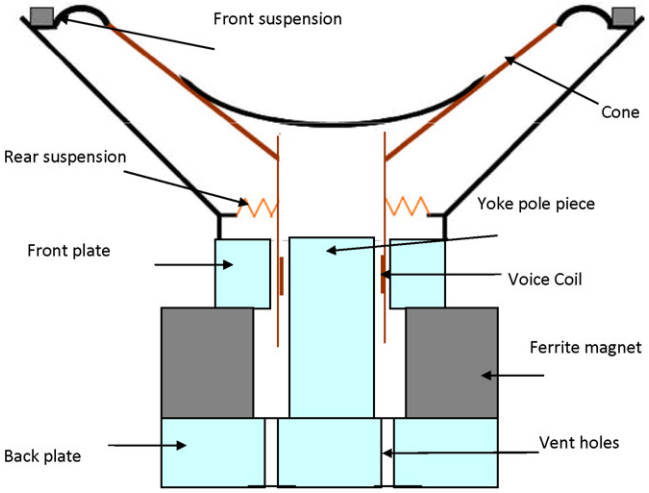

Fig. 2. Schematic of a loudspeaker type alternator.

high displacement, high velocity coil. This causes high air velocity through the vents and high aerodynamic losses. Increasing the size of the vent holes reduces the magnetic path area and ultimately compromises the electrical efficiency. By changing the topology to a Halbach array as shown in Fig. 5, this limitation is removed. However, it does mean that the waveform changes polarity during the cycle and if the coil is allowed to move outside the magnetic gap, non-sinusoidal waveforms result. As discussed earlier this is not an issue for the linear alternator concept.

It is common practice to represent the mechanical and acoustic components as equivalent electrical components. Fig. 3 shows the equivalent electrical circuits for the physical model of the thermo-acoustically driven electromagnetic linear alternator which has already been highlighted in [6,9].

The generated voltage of the alternator is given by:

$$V = \frac{d\phi}{dt} \tag{1}$$

where ϕ is the flux linkage which depends on the magnet and coil parameters and the gap between the magnet and coil. In the general case (e.g. in the case of a Halbach array) the air gap flux density (B_r) will vary with the position. For a uniformly wound coil of height (h_c) centred on $x = y$, the induced voltage is given by

$$V = \frac{l_{cu}}{h_c} \int_{y-(h_c/2)}^{y+(h_c/2)} B_r(x)\, dx\, \frac{dy}{dt} \tag{2}$$

where l_{cu} is the coil length, and $B_r(x)$ is the radial component of the air gap flux density. If the air gap flux density (B_r) is constant over

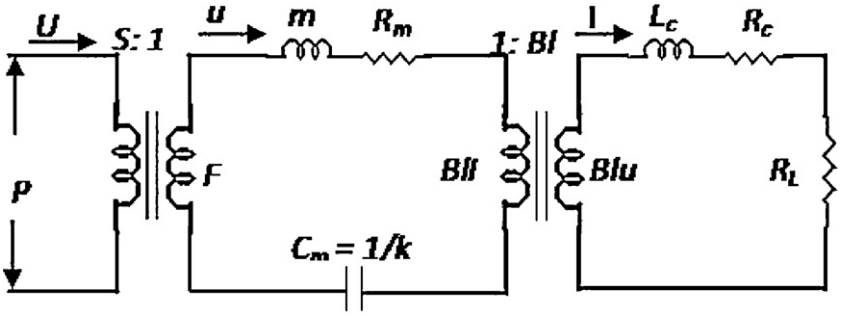

Fig. 3. Equivalent electrical circuit of the thermo-acoustic driven electromagnetic linear alternator.

the coil displacement (which is the normal loudspeaker case) then voltage would be

$$V = \frac{d\phi}{dy}\frac{dy}{dt} = B_r l_{cu}\frac{dy}{dt} \tag{3}$$

The input acoustic power is defined by [7]

$$P_a = \frac{1}{2}[p][U]\cos\theta = \frac{U^2}{2S^2}\left[R_m + \frac{(B_r l_{cu})^2}{R_c + R_L}\right] \tag{4}$$

where S is the cone effective area of the alternator, P is the pressure drop to the alternator, U is the volumetric velocity, $B_r l_{cu}$ is the force factor of the alternator, R_m is the mechanical resistance of the suspension, R_c is the coil resistance, R_L is the load and θ is the angle between pressure (p) and volumetric flow (U). For sinusoidal pressure variation, the generated electrical power (rms) would be [9]

$$P_e = \frac{1}{2}\frac{(B_r l_{cu})^2}{R_c + R_L}u^2 = \frac{1}{2}\frac{U^2}{S^2}\frac{(B_r l_{cu})^2}{R_c + R_L} \tag{5}$$

where $u = \omega y$ is the peak velocity of the cone along the Y axis.

The rms load power is thus

$$P_L = \frac{1}{2}i^2 R_L = \frac{(\omega y B_r l_{cu})^2}{8R_c}\frac{4R_c R_L}{(R_c + R_L)^2} \tag{6}$$

The normalised load power can be defined by

$$\frac{P_L}{(\omega y B_r l_{cu})^2} = \frac{1}{2}\frac{R_L}{(R_c + R_L)^2} \tag{7}$$

If the alternator voice coil displacement is limited to y due to suspension constrain then the maximum output power would be

$$P_{\max} = \frac{(\omega y B_r l_{cu})^2}{8R_c}, \quad \text{when} \quad R_L = R_c \tag{8}$$

It can be seen from Eq. (6) that the load power depends on velocity and the magnet and coil parameters. The velocity or displacement of the cone depends on the effective area of the suspension. For a fixed displacement of the suspension, to increase the generated electrical power the only option is to increase the frequency and/or $(B_r l_{cu})^2/R_c$ factor. A higher frequency increases the velocity as well as voltage for the fixed displacement but decreases thermo-acoustic efficiency of the system; conventional practice for low pressure air thermo-acoustic engines (TAE) is to limit the frequency to less than 120 Hz due to acoustic and regenerator losses [26].

The efficiency can be defined by using Eqs. (4) and (6)

$$\eta_{ae} = \frac{P_L}{P_a} = \frac{(B_r l_{cu})^2 R_L}{R_m(R_c + R_L)^2 + (B_r l_{cu})^2(R_c + R_L)} \tag{9}$$

The maximum efficiency

$$\eta_{\max} = \frac{\beta}{2 + \beta + 2\sqrt{1+\beta}} \tag{10}$$

when $R_L = R_c\sqrt{1 + ((B_r l_{cu})^2/R_c R_m)}$ and $\beta = (B_r l_{cu})^2/(R_c R_m)$.

It can be seen from Eq. (9) that the efficiency depends on magnet and coil parameters and the suspension loss of the system. Fig. 4 shows the calculated normalised load power and efficiency vary with the load resistance, as shown for a typical linear alternator using the force factor ($B_r l_{cu}$) 4.5 T-m. Fig. 4 has been plotted using typical generator parameters such as frequency (100 Hz), displacement (18 mm), mechanical suspension loss (1 N s/m) and coil resistance (0.4 Ω). The maximum efficiency and maximum theoretical power occur at different load resistance. Maximum power is typically limited by the ability of the coil to dissipate its heat loss, so it is usual to operate with load resistances higher than the maximum power case.

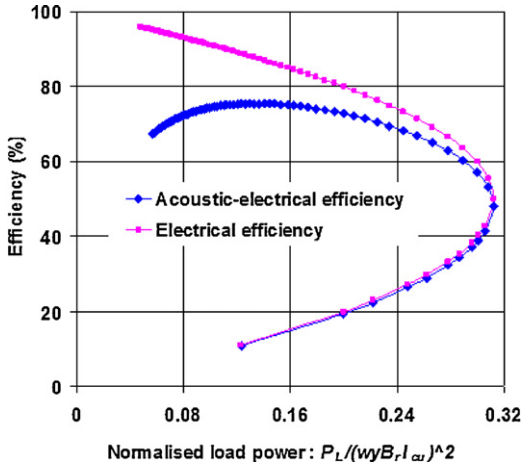

Fig. 4. Normalised load power and efficiency of a typical alternator with resistive load for $B_r l_{cu}$ factor 4.5 T-m.

3. Double Halbach array alternator structure

The basic Halbach array consists of a coaxial pair of three cylindrical permanent magnets [23,24] as shown in Fig. 5. Fig. 6 shows the cross sectional view and dimension/orientation of the basic Halbach array magnets. The outer and inner Halbach array will be magnetized such that the magnetic field is entirely inside the outer cylinder and outside of the inner cylinder. The air gap flux density between the magnet and coil of the double Halbach array is significantly higher than the single permanent magnet and the pumping loss smaller due to larger hole of the inner magnet. The machine is also lighter compared to a traditional back iron machine.

4. Analysis of linear alternator with battery

Since the ultimate goal is to supply power to battery, a rectifier circuit is necessary to convert the ac generated voltage to dc. The Halbach array has a reversal of air-gap flux density between the magnets and coil which require a set of (at least 2) discrete coil to exploit the available flux. The lower the alternator resistance (R_c) the higher the efficiency. Both double and multiple coils configurations have been investigated. Multiple coils can be connected in parallel through individual rectifiers to reduce the in-circuit electrical resistance by minimizing the amount of coil not active in the magnetic field. Fig. 7 shows the schematic of alternator multiple coils configuration with the rectifier circuit. Square or round wire can be used, with square giving better efficiency due to lower resistance in a given coil footprint. The coil resistance of the wire-wound coil is expressed by

$$R_c = \frac{\rho_{cu} N l}{A_{wire}} = \frac{\rho_{cu} l_{cu}^2}{2\pi r_{coil} k_{cu} A_{coil}} = \frac{\rho_{cu} l_{cu}^2}{2\pi r_{coil} k_{cu} h_{coil} t_{coil}} \tag{11}$$

where N is the number of turns, l is the coil mean length, r_{coil} is the coil radius, k_{cu} is the copper filling factor, ρ_{cu} is the copper resistivity, h_{coil} is the coil height, t_{coil} is the coil thickness and A_{coil} is the coil cross sectional area.

Delivered load current from n number of coils can be calculated using the equation

$$I_{i+}(t) = \sum_{i=1}^{n}\frac{V_i(t) - V_d - V_{battery}}{R_c} \tag{12}$$

$$I_{i-}(t) = -\sum_{i=1}^{n}\frac{V_i(t) - V_d - V_{battery}}{R_c} \tag{13}$$

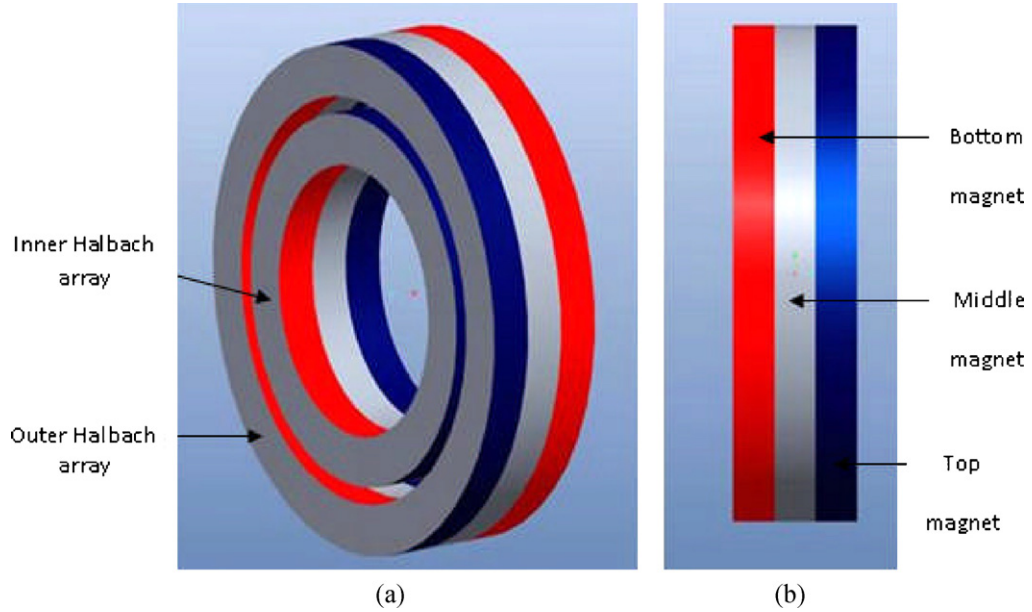

Fig. 5. A three cylindrical magnet double Halbach array structure: (a) isometric view (left) and (b) side view (right). Red represents magnetic north and blue south. (For interpretation of the references to color in this figure legend, the reader is referred to the web version of the article.)

where $V_i(t)$ is the peak generated voltage, $I_{i+}(t)$ is load current from positive peak generated voltage, $I_{i-}(t)$ is load current from negative peak generated voltage, V_d is the diode forward voltage and $V_{battery}$ is the battery voltage.

The average generated power and average load power can be defined by

$$P_e = \sum_{i=1}^{n} \left[\frac{1}{T} \int_0^T |V_i(t) I_{i+}(t)|\, dt + \frac{1}{T} \int_0^T |V_i(t) I_{i-}(t)|\, dt \right] \tag{14}$$

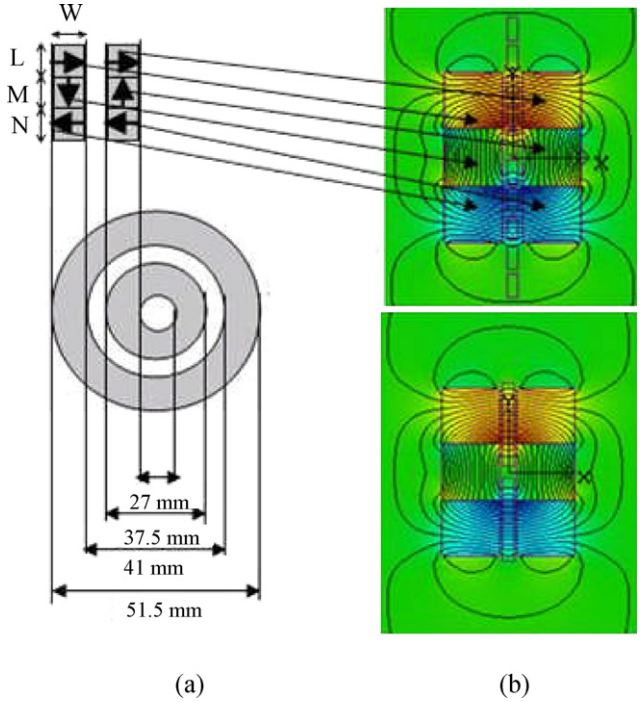

Fig. 6. Schematic of the double Halbach array. (a) NdFeB magnet dimension and orientation. (b) Simulated 2 mm height 10 coils (top) and 7.5 mm height double coil structure alternator.

$$P_L = \sum_{i=1}^{n} \left[\frac{1}{T} \int_0^T |V_{battery} I_{i+}(t)|\, dt + \frac{1}{T} \int_0^T |V_{batteryi} I_{i-}(t)|\, dt \right] \tag{15}$$

Electrical efficiency

$$\eta_e = \frac{P_L}{P_e} \tag{16}$$

5. Simulation results and discussions

The geometry in Fig. 6 with $L = M = N = 5$ mm square magnetic sections meets the cost target, so the first iteration was simulated with these sizes. Later iterations simulated the 2-D magnetic static case to investigate the air-gap flux density of different cross sectional areas of double Halbach array NdFeB magnet structure. The variation of gap flux density (B_x) is plotted along the Y axis as shown in Fig. 8. It can be seen from this graph that magnets with larger cross sections provide higher peak flux density and the curve width becomes wider compare to smaller cross sectional magnet. Fig. 9 shows the variation of air-gap flux density (B_x) along the Y axis with the variation of central magnet length M with fixed $L = N = W = 5$ mm top and bottom magnets. The graph shows that $M = 4$ mm and $M = 5$ mm offer the same peak flux density and similar flux width. The graph also shows that the flux density is not constant over the displacement and is close to sinusoidal in shape. The value of flux density is negligible more than 10 mm away from the central axis. Optimisation of the number of coils to match a fixed voltage load such as a 12 V lead acid battery was carried out using $L = M = N = W = 5$ mm magnet. A 2-D finite element transient simulation (FET) was carried out with different number of coil turns. It can be seen from the gap flux density in Fig. 9 that the peak flux density appears ±3 mm away from the axis centre. In order to generate high voltage, the coils should be placed in this high flux density region when at rest. The upper section of Fig. 6(b) shows a cross section through one side of the magnet with results of the simulated flux lines for 10 off 2 mm high coils between the top and the bottom magnet. The lower section of Fig. 6(b) shows the same section for dual 7.5 mm coils. The coil structure is 1 mm thick and has a gap 0.375 mm from each side of the magnet, giving a magnetic gap of 1.75 mm. Table 1 summarizes the alternator

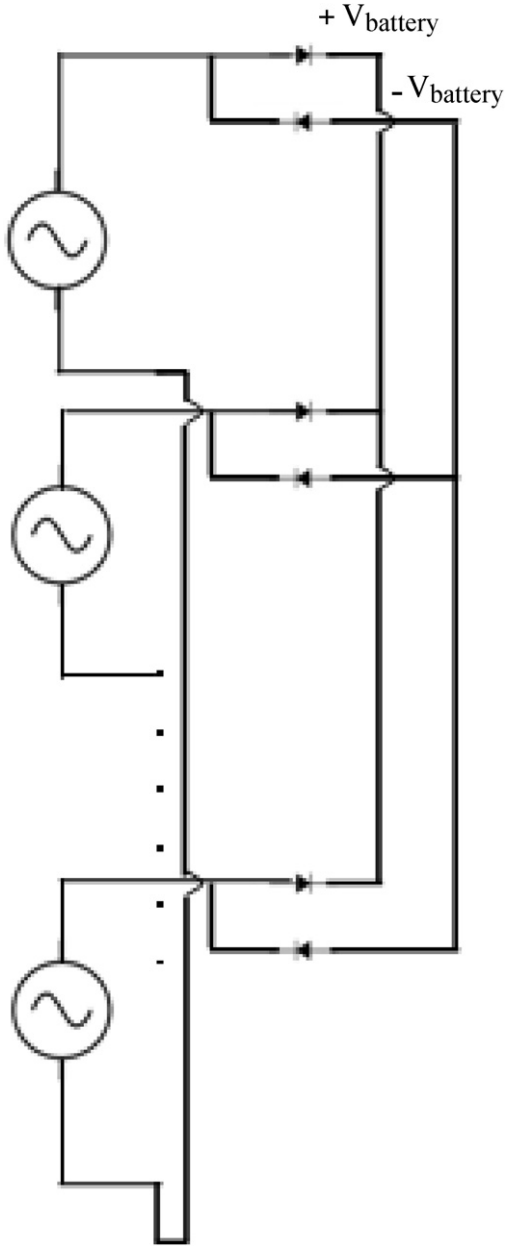

Fig. 7. Schematic of the alternator with the rectifier circuit and the battery load.

parameters. Simulation has been done for 18 mm peak sinusoidal movement from central axis at 100 Hz frequency and using the same wire cross sectional area of the coil. Fig. 10 shows the corresponding voltage shape of different coil heights for the double coil arrangement. Fig. 11 shows the corresponding voltage shape

Table 1
Alternator parameters used in simulation.

Parameters	Dimension
Magnet length: $L = M = N$ (mm)	5
Magnet width: W (mm)	5
Coil outer radius (mm)	40
Coil thickness (mm)	1
Gap between magnet and coil (mm)	0.375
Per turn coil height (mm)	4
Number of turns (N) of 2 mm, 5 mm, 6.5 mm, 7.5 mm and 9 mm coil height	8, 20, 26, 30 and 36
Coil resistance (Ω) of 2 mm, 5 mm, 6.5 mm, 7.5 mm and 9 mm coil height	0.066, 0.17, 0.22, 0.25 and 0.3

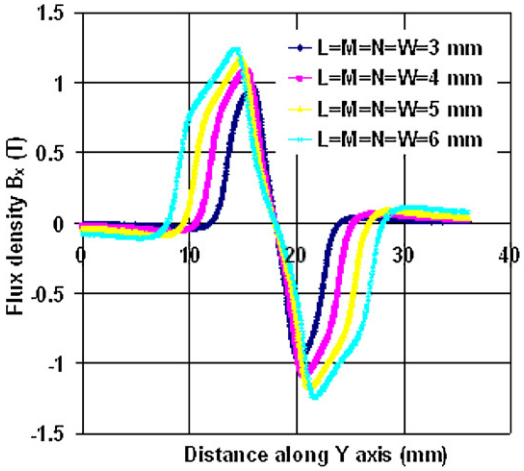

Fig. 8. Variation of flux density (B_x) along the Y-axis of different square size magnets. (For interpretation of the references to color in this figure legend, the reader is referred to the web version of the article.)

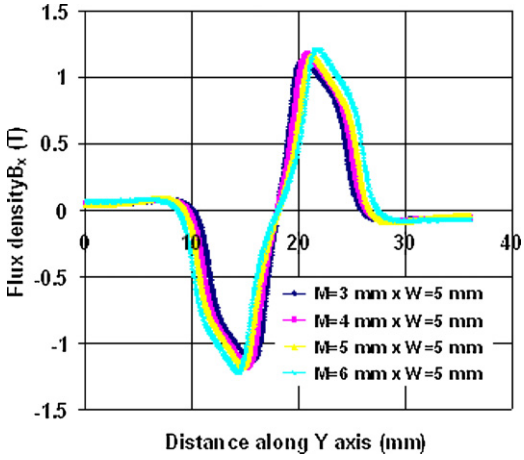

Fig. 9. Variation of flux density (B_x) with the variation of central magnet length for the fixed ($L = N = W = 5$ mm) size top and bottom magnet. (For interpretation of the references to color in this figure legend, the reader is referred to the web version of the article.)

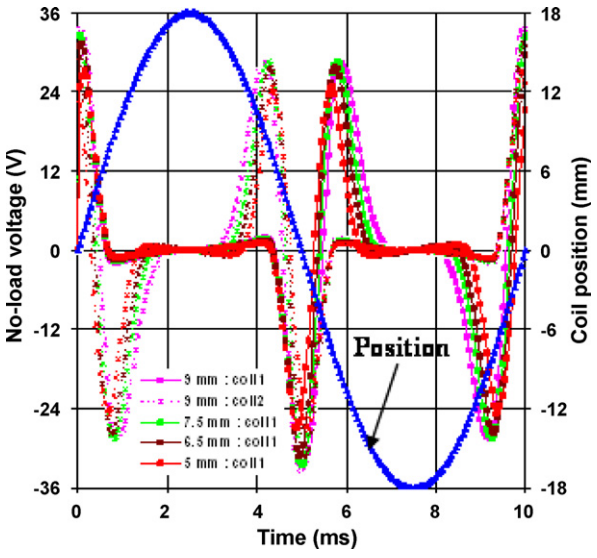

Fig. 10. No-load voltage of the different height double coils and $L = M = N = W = 5$ mm magnet alternator. (For interpretation of the references to color in this figure legend, the reader is referred to the web version of the article.)

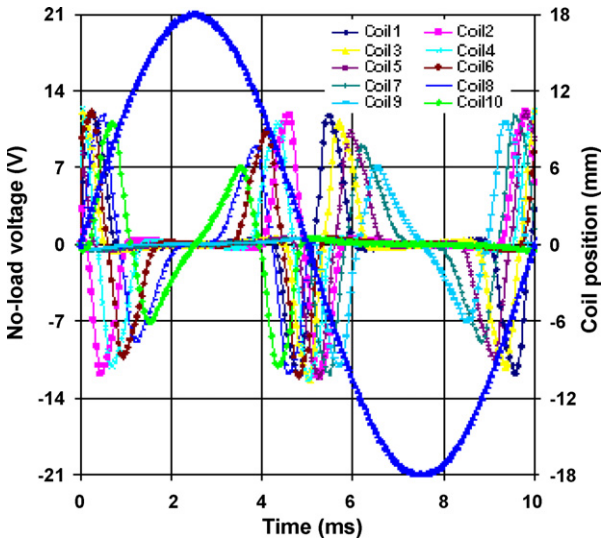

Fig. 11. No-load voltage of 2 mm coil height 10 discrete coils $L = M = N = W = 5$ mm magnet alternator. (For interpretation of the references to color in this figure legend, the reader is referred to the web version of the article.)

of the 10 coils 2 mm coil height. It can be seen from the graph that the voltage is not sinusoidal due to the varying air-gap flux density.

5.1. Performance in battery charging application

The average load power and electrical efficiency of various coil arrangements was calculated for different battery voltages using Eqs. (15) and (16), respectively. The calculated load power and electrical efficiency has been plotted against the ratio of battery voltage ($V_{battery}$) to generated peak voltage (V_i) of the alternator as shown in Fig. 12. In double coil arrangement it can be seen that 7.5 mm height coil will deliver the highest power and efficiency compared to other coils. However the electrical efficiency is increased with the increasing load voltage which obviously delivers the low current at the expense of a reduction of power output and low power loss of the coil. It can also be seen that all the coils deliver the maximum power when the voltage ratio $V_{battery}/V_i$ is close to 0.4 and

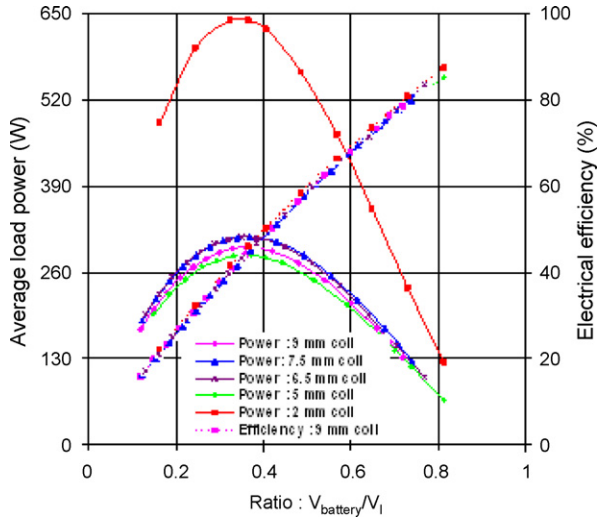

Fig. 12. Load power and efficiency with the variation battery load voltage to peak generated voltage ratio of different height double coil and 2 mm coil height multiple coils alternator. (For interpretation of the references to color in this figure legend, the reader is referred to the web version of the article.)

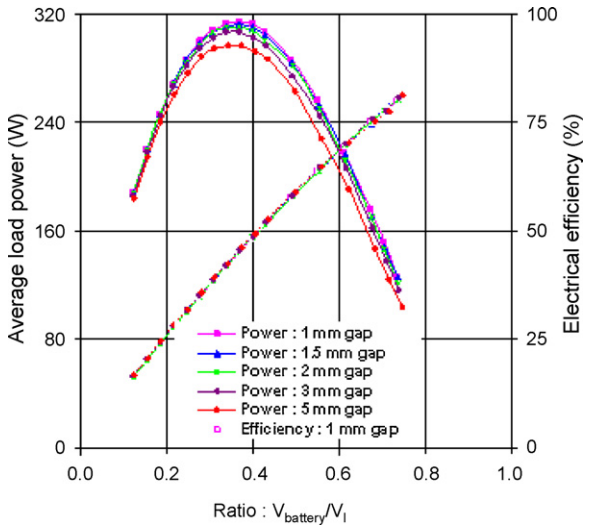

Fig. 13. Load power and electrical efficiency of the 7.5 mm height coil using 30 turns at different positions. (For interpretation of the references to color in this figure legend, the reader is referred to the web version of the article.)

a voltage ratio of 0.65 is required to achieve 70% electrical efficiency. Although the 2 mm coils offer higher levels of total power output, a double coil arrangement is preferred from the cost point of view. In order to understand the optimum position of the 7.5 mm height coil, further simulations have been carried out when the coil is placed ±0.75 mm, ±1 mm, ±1.5 mm and ±2.5 mm away from the central axis to keep the gap 1.5 mm, 2 mm, 3 mm and 5 mm between the coils respectively. The average load power and electrical efficiency of the 7.5 mm height coil for different positions have been plotted with the variation of battery voltage ($V_{battery}$) to peak generated voltage (V_i) ratio as shown in Fig. 13. The graph clearly indicates that the maximum power is transferred to load when the voltage ratio is close to 0.4 and the optimum position of the coil is between ±0.5 mm and ±0.75 mm away from the central axis. Since the SCORE project requires a 150 W deliverable low cost linear alternator and the ultimate goal is to charge the 12 V lead acid battery, the double coil structure with a low number of coil turns would be beneficial.

6. Experimental results of the tested prototype

In order to verify the theory, the moving coil double Halbach array alternator has been built and tested. Fig. 6(a) shows the schematic of the double halbach array NdFeB magnet dimensions and its magnet orientation. The top and bottom magnets are radially magnetized and the middle magnets are vertically magnetized. Since the radial orientation magnet is not commercially available, NdFeB metal sheet has been purchased and cut into eight segments using a wire eroding machine. Each segment was then magnetized in the radial direction. Afterwards all the segments are glued together to form the radially magnetized magnets. Fig. 14 shows the tested prototype fitted into a PVC pipe and Table 2 explains the magnet and coil parameters of the alternator. The coil former is attached to the free end of the 16 segments trapezoidal shape suspension as shown in Fig. 15. The coil and suspension can vibrate up and down linearly when an external force is applied to the alternator coil, the voltage will then be induced at the coil terminals. The suspension has been made from low-loss steel spring material which gives higher efficiency. The segmented suspension will allow large excursions and the gap between segments has been blocked using latex material to reduce the pumping loss of the system.

Fig. 14. Tested prototype of the double Halbach array alternator.

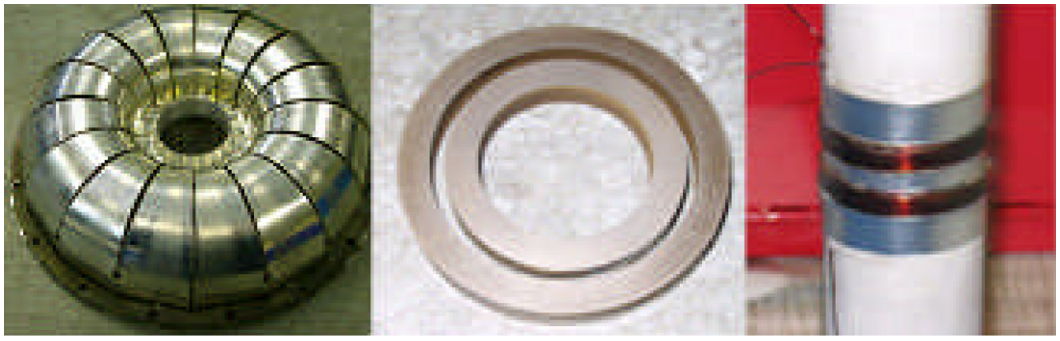

Fig. 15. Alternator: (a) suspension, (b) double Halbach array magnet, and (c) coil.

The mechanical quality factor has been measured at free air using Thiele parameters [27]

$$Q_m = f_n \frac{\sqrt{(Z_{res}/R_c)}}{f_2 - f_1} \tag{17}$$

where, f_n is the free air resonant frequency, Z_{res} is the resonant frequency impedance, R_c is the coil resistance, f_2 and f_1 are the upper and lower −3 db cut-off frequency. The measured mechanical quality factor is 81 at 93 Hz resonant frequency which is significantly higher compare to a typical low cost commercial B&C 6PS38 [28] loudspeaker's mechanical quality factor (Q_m = 11). The mechanical resistance of the alternator suspension can be calculated using the following equation:

$$R_m = \frac{m\omega_n}{Q_m} \tag{18}$$

The suspension resistance (R_m) of the tested prototype is 1.47 N s/m which is still high compared to a low cost B&C 6PS38 commercial loudspeaker (R_m = 0.6) due to the higher moving mass and higher frequency of the alternator. In order to understand the voltage and efficiency of the alternator, the experiment has been carried out using a two microphone method [28]. The acoustic pressure and phase angle between the pressure transducer signals were measured using PCB pressure transducers and a lock-in amplifier. The acoustic power absorbed by the alternator diaphragm has been calculated using Eq. (3) of [29]

$$P_a = \frac{1}{2} \frac{AP_1P_2}{(2\pi f \rho d)} \sin\theta \tag{19}$$

Table 2
Magnet and coil parameters of the tested prototype.

Parameters	Dimension
Magnet length and width (mm)	5 and 5
Coil outer radius and thickness (mm)	40 and 1
Gap between magnet and coil (mm)	0.375
Coil width (mm)	7.5
Number of coil turns (N)	17
Each coil resistance (Ω)	0.5
Free air resonant frequency (Hz)	93
Moving mass (g)	204

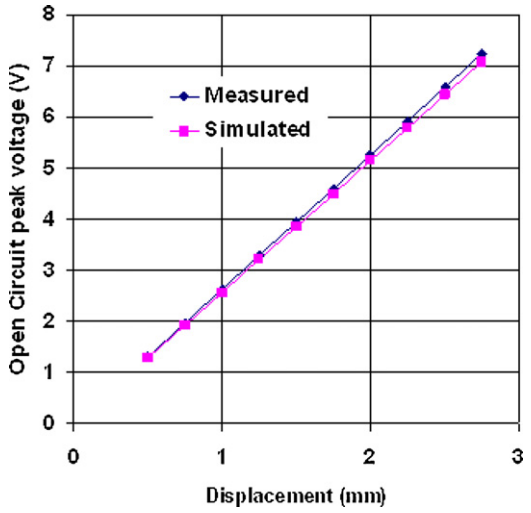

Fig. 16. Measured and simulated open circuit voltage of the alternator.

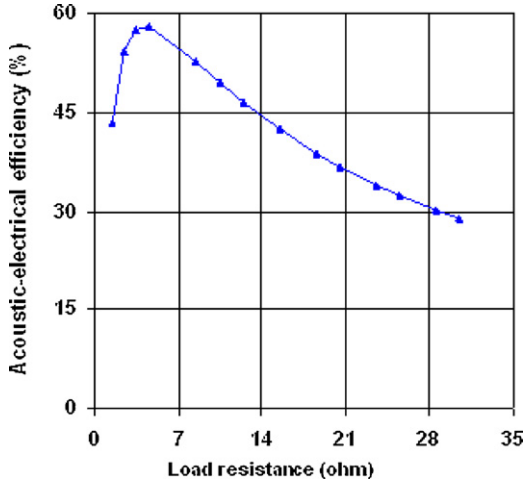

Fig. 17. Derived acoustic-electrical efficiency vs load.

where A is the area of pipe/diaphragm, P_1 and P_2 are the pressure magnitudes, θ is the phase angle, ρ is the air density, and d is the distance between the sensors. The alternator output voltage and diaphragm displacement has been measured using a power analyzer and a laser displacement sensor. The alternator has been driven by the loudspeaker at a fixed input voltage level (6 V) and frequency (93 Hz) with the different input powers level. In order to see the validation of the model, the measured open circuit voltage (coil series connected) of the alternator has been compared with the simulated voltage for different displacement. It can be seen from Fig. 16 that the measured voltage agrees well with the simulated voltage.

The output electrical power has been calculated from the measured voltage and current passing the load resistor; and the input acoustic power has been calculated according to the pressure amplitudes and phase angles from the two pairs of sensors for different load resistances. Efficiencies were derived from early Q and resonant frequency measurements. Direct measurement of efficiency was not possible as the suspension developed progressive cracking during testing causing losses due to fretting of the broken segments. This fretting is likely to account for the derived efficiency 57% being lower than the calculated value of 70%. The derived acoustic-electrical efficiency has been plotted against the load resistance as shown in Fig. 17. The derived efficiency has been calculated according to Eq. (8) using measured Bl, R_m, R_c and R_L values. According to Eq. (8) the acoustic-electrical efficiency depends on the motor parameters and the mechanical suspension loss. However the suspension loss could vary with the material properties, applied frequency, and displacement of the suspension [30–35]. It is necessary to optimise the magnet and coil parameters and the suspension needs to be made from the low loss reliable spring material in order to achieve the high efficiency of the alternator. The low suspension loss definitely provides high displacement as well as high power and high quality factor of the alternator at resonant frequency operation.

7. Conclusions

This paper presents the design issues of the linear alternator for SCORE project and discusses the advantages of the double Halbach array alternator structure over the commercial loudspeaker from the cost and efficiency perspective. The theoretical analysis of the linear alternator with rectifier circuit is described. Finite element simulation results of the double and multiple coils Halbach array alternator structure have been shown and the simulation results clearly indicate that double coil structure with the smaller number of turns would be a suitable option for this project. The calculation results also show that $V_{battery}/V_n$ voltage ratio needs to be more than 0.65 in order to achieve more than 70% electrical efficiency. The measured results of the tested prototype showed that the quality factor of the alternator suspension is significantly high and maximum 57% acoustic-electrical efficiency was derived. The experiment has been done from the low input driving power which obviously gave the low excursion of the suspension and low output power of the alternator. In future it is necessary to see the output power and efficiency of the alternator with the battery load circuit for ±18 mm displacement of the coil.

Acknowledgments

The Score project www.score.uk.com is funded by EPSRC, the UK Engineering and Physical Research Council. Thanks to the Score partners, Professor Chris Lawn, Dr. Catherine Gardner QMUL, Dr. Keith Pullen, Dr. Ron Dennis City University London, and Dr. Teo Sanchez from Practical Action.

References

[1] www.score.uk.com.
[2] www.undp.org.
[3] M. Krishnan, W. Behn, P. Hoke, S. Garrett, Biomass cook stoves: impact on global warming and women and children's health, in: ASEAN-US Next-Generation Cook Stove Workshop, 2009.
[4] P.H. Riley, C. Saha, C.M. Johnson, Designing a low cost electricity-generating cooking stove, IEEE Technology and Society Magazine (Summer) (2010).
[5] Practical Action Field Trial #1 in Nepal and Kenya reports, http://www.score.uk.com/research/default.aspx.
[6] J. liu, S. Garrett, Characterization of a small moving magnet electrodynamic linear motor, Journal of Acoustical Society of America 118 (October (4)) (2005).
[7] R. Scott Wakeland, Use of electrodynamic drivers in thermo-acoustic refrigerators, Journal of Acoustical Society of America 107 (February (2)) (2000).
[8] C.M. Johnson, P.H. Riley, C.R. Saha, Investigation of a thermo-acoustically driven linear alternator, in: U21 Energy Conference, Birmingham, UK, September, 2008.
[9] Z. Yu, S. Backhaus, A. Jaworski, Design and Testing of a Travelling Wave Looped Tube Engine for Low Cost Electricity Generators in Remote and Rural Areas, American Institute of Aeronautics and Astronautics, 2009.
[10] M. Petach, E. Tward, S. Backhaus, Design of a High Efficiency Power Source (HEPS) Based on Thermoacoustic Technology, Los Alamos National Laboratory, Condensed Matter and thermal Physics Group, 2004.
[11] G. Swift, Thermoacoustics: A Unifying Perspective for Some Engines and Refrigerators, Los Alamos National Laboratory, Condensed Matter and thermal Physics Group, 2001.
[12] D.G. Holmberg, G.S. Chen, Thermal modelling and performance analysis of a thermoacoustic refrigerator, Journal of Acoustical Society of America 114 (August (2)) (2003).

[13] C. Herman, Z. Travnicek, Cool sound: the future of refrigeration? Thermodynamic and heat transfer issues in thermoacoustic refrigeration, Heat and Mass Transfer 42 (2006) 492–500.
[14] W.V. Slaton, J.C.H. Zeegers, Thermoelectric power generation in a thermoacoustic refrigerator, Applied Acoustics 67 (2006) 450–460.
[15] P.S. Spoor, J.A. Corey, A novel method for controlling piston drift in devices with clearance seals, in: Cryocoolers 13, Springer Science and Business Media, Inc., New York, 2004.
[16] T. Biwa, Y. Ueda, T. Yazaki, U. Mizutani, Work flow measurements in a thermoacoustic engine, Cryogenics 41 (2001) 305–310.
[17] L. Erchang, W. ZangHua, D. Wei, L. ShanFeng, Z. Yuan, A 100 W-class travelling-wave thermo-acoustic electricity generator, Chinese Science Bulletin 53 (May (9)) (2008) 1453–1456.
[18] I. Boldea, S.A. Nasar, Permanent-magnet linear alternators. Part II. Design guidelines, IEEE Transactions on Aerospace and electronic Systems 23 (1) (1987) 79–82.
[19] W. Cawthorne, P. Famouri, N. Clark, Integrated design of linear alternator/engine system for HEV auxiliary power unit, in: IEEE International Conference on Electric Machines and Drives (IEMDC), 2001, pp. 267–274.
[20] J. Wang, M. West, D. Howe, H.Z.-D. La Parra, W.M. Arshad, Design and experimental verification of a linear permanent magnet generator for a free-piston energy converter, IEEE Transactions on Energy Conversion 22 (2) (2007) 299–305.
[21] J. Faiz, B. Rezaeealam, S. Yamada, Reciprocating flux-concentrated induction generator for free-piston generator, IEEE Transaction on Magnetics 42 (September (9)) (2006).
[22] J. Borwick, Loudspeaker and Headphone Handbook, 2nd ed., Focal Press.
[23] K. Halbach, Design of permanent multipole magnets with oriented rare earth cobalt material, Nuclear Instruments and Methods 169 (1) (1980) 1–10, doi:10.1016/0029-554X(80)90094-4, ISSN: 0029-554X.
[24] J. Seok, Choi, J. Yoo, Design of a Halbach magnet array based on optimization techniques, IEEE Transactions on Magnetics 44 (October (10)) (2008).
[25] B.T. Merritt, R.F. Post, G.R. Dreifuerst, D.A. Bender, Halbach array motor/generators—a novel generalised electric machine, in: Halbach Festschrift Symposium, Berkeley, CA, February 3, 1995.
[26] F. Formosa, G. Despesse, Analytical model for Stirling cycle machine design, Energy Conversion and Management 51 (2010) 1855–1863.
[27] http://online.physics.uiuc.edu/courses/phys498pom/Student_Projects/Spring01/PPoongbunkor/Piya_Poongbunkor_TS.pdf.
[28] http://www.bcspeakers.com/PDF/PRD/186.pdf.
[29] A.M. Fusco, W.C. Ward, G.W. Swift, Two-sensor power measurements in lossy ducts, Journal of Acoustical Society of America 84 (1992) 2229–2235.
[30] C.R. Saha, T. O'Donnell, H. Loder, S. Beeby, J. Tudor, Optimization of an electromagnetic energy harvesting device, IEEE Transaction on Magnetic 42 (October (10)) (2006).
[31] T. O'Donnell, C. Saha, S. Beeby, J. Tudor, Scaling effects for electromagnetic vibrational power generator, Journal of Microsystem Technology (November) (2006).
[32] X. Zhang, W.C. Tang, Viscous air damping in laterally driven microresonators, in: IEEE Proceedings on MEMS Workshop, 1994, pp. 199–204.
[33] R. Liftshitz, M. Roukes, Thermoelastic damping in micro and nanomechanical systems, Physical Review B 61 (February (8)) (2000) 5600–5609.
[34] C. Zener, Internal friction in solids. 1. Theory of internal friction in reeds, Physical Review 52 (1937) 230–235.
[35] J. Yang, T. Ono, M. Esashi, Energy dissipation in sub-micrometer thick single crystal silicon cantilevers, Journal of Micromechanical Systems 11 (6) (2002) 775–783.

Biographies

Chitta R. Saha received his B.Eng. in Electrical and Electronic Engineering from Bangladesh University of Engineering and Technology (BUET) in 2000 and M.Eng.Sc. degree in Microelectronic Engineering from National Microelectronic Research Centre (NMRC), University College Cork (UCC), Ireland in 2003. In 2008 he received his Ph.D. from UCC in the area of electromagnetic energy harvester for wireless sensor module applications. He is currently a research associate on SCORE (www.score.uk.com) project in the Department of Electrical and Electronic Engineering, Nottingham University, UK. Current research interests include design and modelling of energy harvesting applications, alternator, thermo-acoustic technology and power conversion circuits.

Paul H. Riley, B.Sc. (Hons) is a Chartered Engineer, Fellow of the Institution of Engineering and Technology, Fellow Royal Society for the Encouragement of Arts, Manufactures and Commerce and is a Member of the Institute of Directors. He is the current Score Project Director. Under his technical and administrative leadership, Score has produced over 28 journal and conference papers (www.score.uk.com). He created the Score Community and was awarded a TSB funded KTS in 2010 and a KTP with Warrior Stoves this year. He also leads the Score Centre Indian-subcontinent knowledge transfer project that has setup centres at BUET (Bangladesh) and an NGO called Mansha in Jaipur (India). At Rolls Royce (Aerospace), he managed many £multi-million and international projects and was pivotal in improving the reliability of engine-borne electronic control systems; he approved the electronic-engine-control certificate for the RB211 535 E4, which became the most reliable aero-engine in the world. He is an influential speaker and has presented at world-wide events at all levels. Spede was a £2M research project that gained "approaching world class and outstanding" from an EPSRC independent peer review. This 3-university, 3-industrialist consortium was project managed by Paul who exploited the results of the research both within Rolls Royce and externally. He was main board Technical Director of Ramtech Electronics Limited where he reduced manufacturing costs by 28%.

John Paul received the M.Eng.Sc. and the Ph.D. degrees in Electrical and Electronic Engineering from the University of Nottingham, U.K. in 1994 and 1999 respectively. His Ph.D. dissertation involved the application of signal processing and control system techniques to the simulation of general properties in time domain TLM. He is currently employed as a Research Fellow with the George Green Institute for Electromagnetics Research at the University of Nottingham. Research interests are in the application of signal processing techniques for advanced material modelling in time domain computational electromagnetics and the simulation of the complete systems for electromagnetic compatibility studies.

Dr. Zhibin Yu obtained his B.Eng. in Engineering of Cryogenics and Refrigeration from Huazhong University of Science and Technology (China) in 2000. He obtained his Ph.D. in Thermal Energy Systems from Technical Institute of Physics and Chemistry, Chinese Academy of Sciences (China) in 2005. He is currently a Postdoctoral Research Associate working in the University of Leicester (UK). His research interests include: thermoacoustic energy conversion technology and its application for energy recovery from waste heat sources, cryogenic refrigeration, high-efficiency heat pump technologies, and optical diagnostic technique for both fundamental and applied research in thermal and fluid systems.

Artur J. Jaworski obtained his M.Sc. in 1991 from the Warsaw University of Technology and Ph.D. in 1996 from Imperial College of Science, Technology and Medicine in London. He is currently Professor of Engineering and Head of the Thermofluids Research Group in the Department of Engineering, University of Leicester, UK. His interests in Thermoacoustic Technologies date back to 1999. He has been the first UK researcher seriously funded in this discipline by the UK Engineering and Physical Sciences Research Council (EPSRC) and pioneered a wider UK interest in this research field. Between 2004 and 2009 has held a prestigious EPSRC Advanced Research Fellowship in thermoacoustics. His interests span from the fundamentals of heat transfer and fluid flow to practical implementations of thermoacoustic devices.

C Mark Johnson received the BA degree in engineering and the PhD degree in electrical engineering from the University of Cambridge, UK, in 1986 and 1991 respectively. From 1992 to 2003 he was a Lecturer and later Reader at the University of Newcastle where he led research into Silicon Carbide electronics. In 2003, he was appointed as Rolls-Royce/RAEng Research Professor of Power Electronic Systems at the University of Sheffield and in 2006 he was appointed to a personal chair at the University of Nottingham, where he leads research into power electronics integration and energy systems. He is PI for the UK Engineering and Physical Sciences Research Council (EPSRC) funded Score project and is a member of the executive committee of the UK Innovative Electronics Manufacturing Research Centre (IeMRC).